pH-Dependence of Extrinsic and Intrinsic H^+-Ion Mobility in the Rat Ventricular Myocyte, Investigated Using Flash Photolysis of a Caged-H^+ Compound

Pawel Swietach,* Kenneth W. Spitzer,† and Richard D. Vaughan-Jones*
*Burdon Sanderson Cardiac Science Centre, Department of Physiology, Anatomy and Genetics, Oxford University, Oxford, United Kingdom; and †Nora Eccles Harrison Cardiovascular Research and Training Institute, University of Utah, Salt Lake City, Utah

ABSTRACT Passive H^+-ion mobility within eukaryotic cells is low, due to H^+-ion binding to cytoplasmic buffers. A localized intracellular acidosis can therefore persist for seconds or even minutes. Because H^+-ions modulate so many biological processes, spatial intracellular pH (pH_i)-regulation becomes important for coordinating cellular activity. We have investigated spatial pH_i-regulation in single and paired ventricular myocytes from rat heart by inducing a localized intracellular acid-load, while confocally imaging pH_i using the pH-fluorophore, carboxy-SNARF-1. We present a novel method for localizing the acid-load. This involves the intracellular photolytic uncaging of H^+-ions from a membrane-permeant acid-donor, 2-nitrobenzaldehyde. The subsequent spatial pH_i-changes are consistent with intracellular H^+-mobility and cell-to-cell H^+-permeability constants measured using more conventional acid-loading techniques. We use the method to investigate the effect of reducing pH_i on intrinsic (non-CO_2/HCO_3^- buffer-dependent) and extrinsic (CO_2/HCO_3^- buffer-dependent) components of H_i^+-mobility. We find that although both components mediate spatial regulation of pH within the cell, their ability to do so declines sharply at low pH_i. Thus acidosis severely slows intracellular H^+-ion movement. This can result in spatial pH_i nonuniformity, particularly during the stimulation of sarcolemmal Na^+-H^+ exchange. Intracellular acidosis thus presents a window of vulnerability in the spatial coordination of cellular function.

INTRODUCTION

Regulation of intracellular pH (pH_i) is essential for the maintenance of normal cellular function. In the mammalian heart, modest displacements of pH_i from its resting level of 7.1–7.2 occur physiologically, for example during increases in cardiac workload (1,2) and during extracellular acid-base disturbances (3,4). Because of the high chemical reactivity of H^+-ions, notably with intracellular proteins, such displacements affect the electrical (5) and contractile (4, 6) behavior of the heart, and must eventually be corrected via regulatory processes. Larger displacements of pH_i occur during clinical disorders such as myocardial ischemia (7) where they induce severe contractile dysfunction (6,8) and arrhythmia (9).

The regulation of cardiac pH_i is achieved by means of ion transport proteins, which translocate H^+, OH^-, and HCO_3^- ions across the sarcolemma. Their ability to regulate pH_i depends on adequate H^+-ion mobility within the cytoplasmic compartment. H^+-diffusion, however, is severely restricted because of high intracellular H^+-buffering (~50,000, equivalent to an intracellular buffering capacity of ~50 mM). Most of this buffering occurs at histidine residues on intracellular proteins that, because of their large size, exhibit low mobility. We have shown that adequate H^+-mobility within ventricular myocytes is furnished by a population of lower molecular weight diffusible buffers, such as the histidyl dipeptides acetylcarnosine, acetylanserine, and homocarnosine (10). These chaperone H^+-ions around the cell on a mobile buffer shuttle, thereby enabling the spatial regulation of pH_i. One important feature of the shuttle is that, although it distributes H^+-ions within the cell, it results in an effective H_i^+-mobility (D_H^{app}, the apparent H^+-diffusion coefficient) more than two orders of magnitude lower than in unbuffered solution (11). Another important feature is that, when pH_i decreases, many of the diffusible buffers approach saturation by H^+-ions, causing a further fall in H_i^+-mobility (12). Low H_i^+-mobility can result in significant spatial nonuniformity of cytoplasmic pH_i, particularly when large fluxes of acid occur across the sarcolemma (13).

In addition to intrinsic buffers such as histidyl dipeptides, the major extrinsic buffer system, CO_2/HCO_3 (carbonic buffer), can also shuttle H^+-ions spatially within a cell, particularly when catalyzed endogenously by the enzyme, carbonic anhydrase (14–16). It is not known, however, if this component of the buffer-shuttle is modulated by changes of pH_i in a manner similar to that observed for the intrinsic shuttle. In this work we have therefore examined the relative roles of extrinsic and intrinsic buffer in setting H_i^+-mobility in the ventricular myocyte, over a range of pH_i values. This permits an assessment of their physiological importance in the spatial regulation of pH_i.

To assess H_i^+-mobility, a local rise of $[H^+]_i$ is typically induced in one region of the cytoplasm and its spatial dissipation imaged confocally using an intracellular pH-fluorophore, such as carboxy-SNARF. Current methods for locally displacing pH_i include H^+ loading from an acid-filled

Submitted September 1, 2006, and accepted for publication September 25, 2006.

Address reprint requests to Richard D. Vaughan-Jones, E-mail: richard.vaughan-jones@physiol.ox.ac.uk.

0006-3495/07/01/641/13 $2.00

doi: 10.1529/biophysj.106.096560

patch-pipette (11), and local microperfusion of extracellular membrane-permeant acidic molecules such as CO_2 or acetic acid (17,18). Such approaches can be technically demanding and may not be suitable for all cell-types. We have therefore tested a novel method for introducing H^+-ions into a cell, by uncaging them from the membrane-permeant, proton-donor compound, 2-nitrobenzaldehyde (NBA), using ultraviolet (UV) flash-photolysis. Apart from a brief report for a neuronal preparation (19), this technique has not been applied previously in intact cells. In this work, we explore its potential in isolated ventricular myocytes. We assess the suitability of NBA for local and whole-cell intracellular proton uncaging, we estimate the photolytic efficiency of the process, and we gauge its usefulness for measuring H_i^+-mobility in single cells, and cell-to-cell H^+-permeability in cell-pairs. Having validated the technique, we then use it to elucidate the pH_i-sensitivity of H_i^+-shuttling via extrinsic and intrinsic buffer.

METHODS

Cell isolation

Cardiac myocytes were isolated from ~300 g Sprague-Dawley rats (killed by cervical dislocation in accordance with UK Home Office guidelines) using a combination of mechanical and enzymatic (0.24 mg/ml Blendzymes III, Roche, UK) dispersion (11,16,20). Cells were stored in DMEM culture medium (Sigma, UK) at room temperature.

Solutions

HEPES-buffered normal Tyrode (NT) solution contained (in mM): NaCl (135), KCl (4.5), HEPES (20), $CaCl_2$ (2), $MgCl_2$ (1), glucose (10). Solution pH was adjusted to 7.4 using 4 M NaOH. CO_2/bicarbonate-buffered NT contained (in mM): NaCl (120), KCl (4.5), $NaHCO_3$ (22), $CaCl_2$ (2), $MgCl_2$ (1), glucose (10). Solution pH was adjusted to 7.4 by continuously bubbling with 5% CO_2. Where indicated, 1 mM NBA (from 1 M stock dissolved in methanol) was included in solutions. In some experiments with coupled cell-pairs, 60 μM α-glycyrrhetinic acid (αGA) was included in superfusates to block gap junctional channels (20). In other experiments, the enzyme carbonic anhydrase was blocked with 100 μM acetazolamide (ATZ). All chemicals were obtained from Sigma.

Cell superfusion

Experiments were carried out in a 500-μl Plexiglas flow-through chamber with the base made from a thin, glass coverslip. To facilitate cell adhesion, the coverslip was coated before each experiment with 100 μl 0.01% poly-L-lysine (Sigma). After washing away poly-L-lysine, 200 μl of cells in culture medium were applied to the superfusion chamber, mixed with 1.5 μl 1.7 mM solution of an acetoxy-methyl (AM) carboxy-SNARF pH-fluorophore (Molecular Probes, Eugene, OR) in DMSO. For experiments at alkaline or resting pH_i, carboxy-SNARF-1 was used ($pK = 7.5$), whereas at lower pH_i, the recently developed analog, carboxy-SNARF-4F ($pK = 6.4$), was preferred (21). The physicochemical properties of the two dyes (e.g., their membrane permeability, molecular mass and chemical structure) are very similar, differing only by the pK shift in their emission spectra. After 10 min of dye-loading in darkness, cells were continuously supplied with superfusate. When required, two platinum wires along the length of the chamber were used to field-stimulate the cells.

Confocal pH_i imaging

Cells were imaged using an inverted confocal microscope (TCS NT system on a DM IRBE microscope; Leica, Wetzlar, Germany) equipped with a $\times 63$ plano-apochromat, water-immersion objective (NA 1.2) with UV correction. The carboxy-SNARF dyes were excited by the 514-nm line from an Argon laser, and fluorescence emission was measured at 580 $\pm$ 20 nm and 640 $\pm$ 20 nm (line scan speed = 400Hz). The ratio of fluorescence intensity measured at the two wavelengths was converted to pH using calibration curves obtained in separate experiments (22).

H^+-uncaging from NBA

After loading with pH-fluorophore, the cells were then loaded with the H^+-donor compound by including 1 mM NBA in all superfusates. This is highly membrane-permeant, superfusion typically commencing a few minutes before an experiment. Cells loaded with 1 mM NBA for 1 min produced the same magnitude of acid-uncaging as cells loaded for >3 min. When exposed to UV light-flashes at 351 nm from a 20-mW UV laser (Enterprise II Laser; Coherent, CA), NBA undergoes an intramolecular redox reaction (23) giving 2-nitrosobenzoic acid (Fig. 2 *A*). The pK of 2-nitrosobenzoic acid is ~2.2 and so the product is fully dissociated in the physiological pH_i range. Despite photolysis, the intracellular concentration of NBA remained constant owing to continued passive entry from the superfusate. Without electronic zoom, the ROI exposed to UV light could be as large as 150 $\times$ 150 μm (entire field of view) or as small as 5 $\times$ 5 μm (the smallest sweep length). At a pixel resolution of 256 $\times$ 256 and a line-scan speed of 400 Hz, the UV laser dwell-time per pixel was ~10 μs. UV light intensity could be reduced by neutral-density filters to obtain the desired magnitude of intracellular acid-load. Since high-energy laser exposure tends to damage cells, two consecutive UV flashes of lower intensity, separated by 0.95 s (a flash-event), were preferred over a single, higher intensity exposure.

The excitation protocol could be programmed to switch automatically between Argon laser for carboxy-SNARF excitation and acquisition of pH_i data, and UV laser for flash-photolysis. Due to time delays imposed by the changes in microscope optics, the shortest transition time between ''acquisition mode'' and ''photolysis mode'' was 3–4 s.

Presetting starting pH_i

Superfusion with NT stabilizes pH_i at 7.1–7.2. In some experiments, pH_i was preset uniformly to different levels before starting an experiment. To manipulate starting pH_i, cells were prepulsed (24,25) with solutions containing ammonium chloride or sodium acetate (based on NT solutions, with an appropriate reduction in [NaCl] to keep overall osmolarity constant at ~310 mOsm/kg). After the prepulse, cells were returned to NT solutions containing no weak base or weak acid, resulting in an intracellular acidosis or alkalosis, respectively. By varying the dose of acetate (40–80 mM) or ammonium (10–30 mM) and the duration of the prepulse (4–8 min), it was possible to attain any desired pH_i value in the range 6.2–7.8. To clamp the pH_i to the new displaced level, measures were taken to block sarcolemmal acid/base transport pharmacologically or by ion-substitution. Na^+-H^+ exchange (NHE) was blocked by including 30 μM cariporide (Aventis, Germany) in superfusates (26,27). In CO_2/bicarbonate-buffered superfusates, Na^+-HCO_3^- cotransport (NBC) was 90% blocked by 10 μM S0859 (Aventis) (27); in CO_2-free solutions, NBC was not active. In CO_2/bicarbonate-buffered superfusates, acid-loading transporters (Cl^--HCO_3^- exchange and Cl^--OH^- exchange) were blocked by replacing extracellular chloride salts with an equivalent concentration of gluconate salts (with an appropriate rise in total added [Ca^{2+}] from 2 to 8.5 mM to account for the binding of Ca^{2+} to gluconate) (28). In CO_2-free solutions, sarcolemmal H^+-equivalent influx at high pH_i is mediated by Cl^--OH^- exchange (CHE) (25). Because this is kinetically slow (<1 mM/min), no inhibitory measures were taken in experiments that lasted up to 2 min.

Offline data processing

The confocal system produces three stacks of images: a spatial fluorescence map of the cell at 580 nm, a spatial fluorescence map at 640 nm, and the transmission image of the cell. The transmission image is used to describe the cell geometry, whereas the ratio of the fluorescence at 580 nm and 640 nm (after background offsetting) gives a measure of pH_i. Raw data were processed into $[H^+]_i$ time courses, averaged within rectangular ROIs (typically 15–20 μm by 15–20 μm), aligned along the length of the cell (macro written in Scion Image; Scion).

For H^+-loading experiments using serial H^+-ion uncaging, the mean time course of rise of $[H^+]_i$ in each ROI was fitted with an algorithm for two-dimensional H^+-diffusion from a constant source (defined by the UV-flash area). For single cells (16), the diffusion equation was solved over a single reflective compartment, defined by the geometrical boundary of the cell. The fitting procedure was solved using the finite element method, assuming a single value for the apparent intracellular H^+-diffusion coefficient (D_H^{app}) (29). By varying the starting level of $[H^+]_i$ (see above) and restricting each best-fit to a fall in cell-averaged pH_i of <0.3 pH-units, it was possible to discern the pH_i-dependence of D_H^{app}, as described in the Results section. The estimate of D_H^{app} was assigned to a pH_i value equal to the cell-averaged pH_i at the mid-point of acid-loading. Different values for starting $[H^+]_i$ were spaced as closely as 0.05 pH-units.

For experiments where the relaxation of a longitudinal pH_i-gradient was imaged after terminating the local acid-uncaging sequence, $[H^+]_i$ data were fitted to a two-dimensional reflective compartment model with a nonuniform initial condition. The entire relaxation period was used for best-fitting, and the estimate of D_H^{app} was assigned to the cell-averaged pH_i at the midtime of relaxation.

In the case where H^+-uncaging was performed locally in a cell-pair, the two-dimensional diffusion equation was solved (20) over two reflective compartments, coupled across the junctional membrane by a passive permeation flux, described by an apparent permeability coefficient (P_H^{app}). The boundary condition for this junctional membrane was: $H^+\text{-Flux}_{cell1\rightarrow2} = P_H^{app} \times ([H^+]_{cell2} - [H^+]_{cell1})$.

Statistical analysis of data was performed using Student's unpaired *t*-test or by one-factor analysis of variation. The level of significance was set to 5%. Data are presented as mean ± SE.

Measurements of cell-shortening and intracellular Ca^{2+}

Experiments were carried out on an epifluorescence set-up built on a Nikon Diaphot microscope (Nikon, UK). Rat myocytes were AM-loaded with 10 μM of the Ca^{2+}-indicator, Fluo-3 (Molecular Probes). During superfusion with HEPES-buffered NT, cells were electrically field-stimulated (60–70 V, 0.2-ms pulses at 1 Hz from an isolated DC stimulator). Intracellular fluorophore was excited by a Xenon lamp monochromator (Optoscan, Cairn, UK) at 488 nm and Ca^{2+}-sensitive fluorescence >515 nm was measured with a photomultiplier tube. Cell contraction was measured simultaneously using an edge-detection device (Crescent Electronics, UT) that utilized the transmission image of the cell. Data were digitized with a CED 1401plus digitizer (Cambridge Electronic Design, UK) and recorded with Spike2 software (Cambridge Electronic Design). Ca^{2+} data are presented as a ratio, relative to diastolic Ca^{2+} (F/F_0); cell-shortening has been normalized to the control value averaged over the first minute of stimulation.

RESULTS

Effect of 2-nitrobenzaldehyde on excitation-contraction coupling

Isolated myocytes were electrically activated by field stimulation at 1 Hz. Fig. 1, *Aii* and *Bii*, show simultaneous recordings of the evoked Ca^{2+}-transient and cell-shortening before, during, and after a 3-min exposure to 1 mM NBA. The caged H^+-compound did not affect the time course or amplitude of the Ca_i^{2+}-transient (Fig. 1 *A*), and had no influence on peak cell-shortening (Fig. 1 *B*), indicating that it does not disrupt excitation-contraction coupling. In 5 out of 10 cells, however, a reversible slowing of the late phase of relaxation was observed. We did not investigate this phenomenon further as it was not a consistent occurrence, and there was no other detectable effect of NBA. The slowing was most likely due to direct interference of NBA with the myofilaments or the cell's viscoelastic machinery, rather than an influence on intracellular Ca^{2+} dynamics, as relaxation of the Ca^{2+}-transient was unaffected.

When superfused with 1 mM NBA ($n = 10$), myocytes typically remained quiescent and rod-shaped for at least 10 min, whereas, with 5 mM NBA ($n = 10$), cells usually survived for no more than 5 min. At 10 mM NBA, cells rapidly developed membrane blebs and displayed hypercontracture within 1–2 min. NBA was therefore applied at 1 mM in all subsequent experiments.

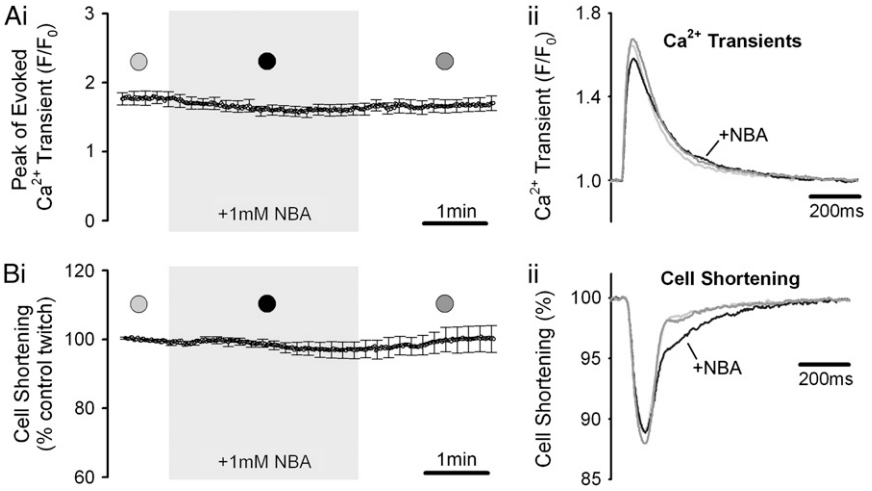

FIGURE 1 Effect of 2-nitrobenzaldehyde on excitation-contraction coupling. Rat myocytes were superfused with HEPES-buffered media and field-stimulated at 1Hz. After a period of pacing (>1 min), cells were exposed to superfusates containing 1 mM NBA. The evoked Ca^{2+}-transient (*A*) and cell-shortening (*B*) were measured simultaneously (mean ± SE; $n = 10$). (*Ai*) Peak systolic Ca_i^{2+}-fluorescence is plotted versus time (peak systolic, *F*, normalized to diastolic Ca^{2+}-fluorescence, F_0). (*Bi*) Mean contraction amplitude (for each experiment, normalized to initial control contraction [averaged over 1 min]) is plotted versus time. (*Aii*) Superimposed time courses of Ca^{2+}-transients from a representative experiment, taken at times indicated in panel Ai. (*Bii*) Superimposed time courses of cell-shortening, taken from same experiment as *Aii*.

Whole-cell flash-photolysis

When UV light is scanned across the entire area of a cell, pH_i should decrease uniformly, provided the intracellular concentration of NBA is uniform. This assumption is likely to hold true because NBA is a membrane-permeant, low molecular-weight solute (151 Da) that is neither charged nor subject to transmembrane transport or metabolism. NBA had no effect on resting pH_i until the cell was exposed to UV light (see Figs. 2 *B*, 4 *Ai*, 5 *Ai*, 6 *A*). Fig. 2 *B* shows data pooled from several experiments where the entire field of view encompassing a cell was exposed to UV flash-events at 0.11 Hz (indicated by the *arrows*), interposed by 2-s periods of pH_i data-acquisition (with 2-frame averaging). Photolytic redox of extracellular NBA did not lead to accumulation of extracellular acid because uncaged protons were washed away by continuous superfusion. H^+-ions uncaged within the cell, however, produced a cumulative fall of pH_i of ~0.65 pH_i units within 3.5 min at 50% laser intensity (*solid circles*). This acid-load was not extruded, as the cell was superfused with a CO_2/HCO_3^--free solution (to inhibit NBC) containing 30 μM cariporide (to inhibit NHE).

The change of pH_i (ΔpH_i) plotted for each flash-event in Fig. 2 *B*, when multiplied by an appropriate value of buffering capacity (16), reveals the quantum of acid uncaged (J_q). Fig. 2 *C* plots J_q as a function of time, for the successive flash-events illustrated in Fig. 2 *B*. J_q is relatively constant, indicating that the quantum was independent of the level of pH_i. Note that the cumulative fall of pH_i plotted in Fig. 2 *B* is curved rather than linear, because pH is a logarithmic function of $[H^+]$, and intrinsic buffering capacity increases as pH_i falls (16,25). Thus, even though H^+-release per flash-event is constant, the resulting ΔpH_i is increasingly attenuated as pH_i falls.

The magnitude of the cumulative acid-load depended on the intensity of UV light, which could be varied by means of neutral density filters. Halving the laser intensity from 50% to 25% (by introducing a higher neutral density filter) reduced the mean acid-loading rate during the flash-sequence (Fig. 2 *B*, *shaded circles*), and halved the quantum of acid released per event (Fig. 2 *C*). J_q could therefore be graded experimentally.

The amplitude and time course of ΔpH_i during a flash-event is shown at higher resolution in Fig. 2 *D*. Here, rat myocytes were exposed to flash-events of different laser

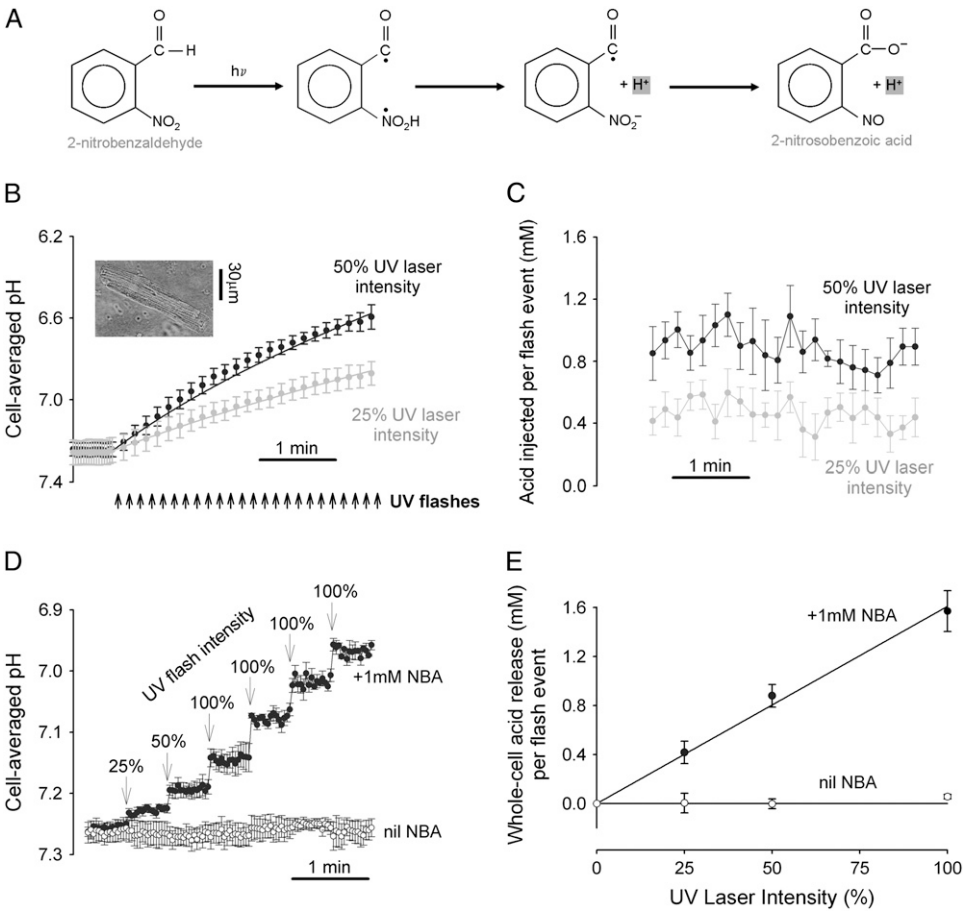

FIGURE 2 H^+-uncaging in whole-cell (*A*). The energy from UV light catalyzes the intramolecular redox between the nitryl and aldehyde group of 2-nitrobenzaldehyde, producing 2-nitrosobenzoic acid which dissociates to its anion and H^+. (*B*) Inset shows rat myocyte superfused with HEPES-buffered NT containing 1mM NBA and 30 μM cariporide. (*Main panel*) repetitive exposure of entire myocyte to UV flash events at 0.11Hz (*denoted by arrows*) produces a cumulative acidification which was monitored in between flash-events using carboxy-SNARF fluorescence: acid-loading rate, 4.16 mM/min at 25% laser intensity (*shaded circles*; $n = 10$) and 8.14 mM/min at 50% laser intensity (*solid circles*; $n = 10$). The continuous curves show model-predictions for constant acid-injection rates into a compartment with a buffering capacity as defined in (16). (*C*) The amount of acid released per flash-event, calculated from the change in pH_i after each flash-event multiplied by the intrinsic buffering capacity ($n = 10$). (*D*) Rat myocytes were superfused with HEPES-buffered NT containing 30 μM cariporide. In some experiments, 1 mM NBA was included in superfusates. Cells ($n = 6$ with NBA, $n = 7$ without NBA) were exposed to a UV flash-event of varying magnitude (25–100% of full power) every 30 s. Between flash events, pH_i was imaged every 2.1 s. (*E*) The stepwise fall in pH_i recorded in D was converted into a measure of acid released per flash-event ($J_{inj} = -\Delta pH \times \beta$), using values for buffering-capacity (β) measured previously (16). This has been plotted as a function of laser intensity. Data points in all panels shown as mean ± SE.

intensity (once at 25%, once at 50%, and then four times at 100% intensity), each followed by a 30-s period of pH_i data acquisition. The superfusates were again HEPES-buffered and contained 30 μM cariporide to inhibit sarcolemmal acid-extrusion. Each flash-event produced a rapid and sustained fall of pH_i, (*solid circles*) whereas the whole sequence induced a series of stepwise decreases of pH_i. The results therefore indicate that H^+-uncaging is both rapid and irreversible. Because of the delay between UV-exposure and pH_i-recording in our apparatus, we were unable to resolve the kinetics of uncaging but, in aqueous solution, it is known to occur within nanoseconds (30). Note that the flash sequence produced no change of pH_i in the absence of NBA (*open circles*), indicating that the source of acid was indeed NBA redox. It also confirms that UV laser-light itself did not influence the fluorescent signal from the pH reporter-dye.

The constancy of pH_i immediately after a flash-event indicates that acid release was uniform along the vertical axis of the cell, and also that the photolytic product, 2-nitrosobenzoic acid, does not flux significantly from the cell (if this happened, the acid-load would be dissipated). Fig. 2 *E* plots the mean quantum of H^+-release as a function of laser intensity. This increases linearly with UV light intensity, reaching 1.6 mM acid released per event for 100% laser power. This represents a quantum yield for an individual UV flash of ~80% (1 flash-event = 2 individual flashes separated by 0.95 s; see Methods). The absence of saturation of acid-release with increasing laser power suggests that NBA photolyzed at the flash site is replenished rapidly i.e., sarcolemmal permeation of NBA is not a rate-limiting factor for intracellular H^+-uncaging.

Regional flash-photolysis: modeling H^+-uncaging protocols

By confining the UV laser-scanning area to a small region of the cell, a local acidosis can be produced. This local pH_i change then drives dissipative H^+-fluxes that obey Fickian diffusion. Two experimental protocols were used to drive these dissipative H^+-fluxes: i), the H^+-load was ramped up locally in a stepwise manner using a prolonged burst of identical flash-events, and the rise of H^+-ion concentration in adjacent regions was monitored between flash-events; and ii), the local H^+-load was established by a shorter rapid burst of flash-events, and its subsequent dissipation upon termination of the burst was monitored. The kinetics of the dissipative H^+-fluxes, whether driven during or after the acid-load, were quantified in terms of an apparent H^+-diffusion coefficient, D_H^{app}.

The validity of the two protocols was explored using a mathematical model, as shown in Fig. 3. In panel *A*, repetitive H_i^+-uncaging at 0.11 Hz (Protocol 1) was simulated at the left end of a rectangular model-cell. For a given value of D_H^{app}, this produces local stepwise increments in $[H^+]_i$, which start to dissipate into neighboring regions. The result is a saw-toothed rise of $[H^+]_i$ averaged within an ROI positioned over the H^+-uncaging region. The time course, however, becomes smoother the more distal the ROI is positioned from the release site. In actual experiments, data acquisition would normally take place at the midpoint between flash-events, as indicated by the solid circles. These points are readily fitted by a two-dimensional diffusion equation (*dashed lines*), taking the same value for D_H^{app}, but assuming a constant localized source of acid-injection at the release-site. We therefore used the simpler, constant-source model (16) when analyzing experimental data obtained with repetitive quantal uncaging.

Fig. 3 *B* illustrates the results of modeling a brief burst of six flash-events and the subsequent relaxation of the pH_i nonuniformity (Protocol 2). The solid symbols represent pH_i at intervals, equivalent to the pH-sampling periods used during experiments (2.1 s), whereas the continuous lines are the full time courses predicted by the model. The relaxation

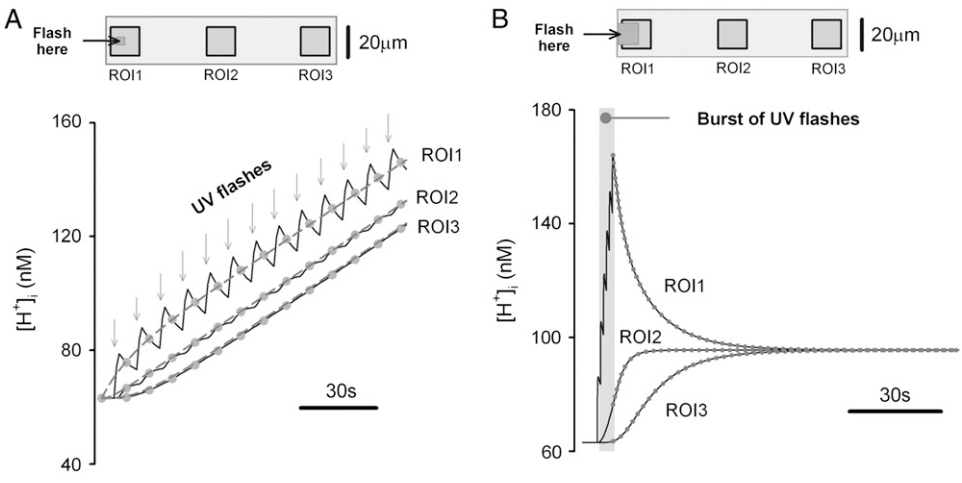

FIGURE 3 Protocols for producing localized acid-loads. A computational model was used to simulate localized H^+-uncaging within a rectangular model-cell (100 × 25 μm) featuring a D_H^{app} of 10^{-6} cm^2/s. (*A*) Protocol 1: simulation of repetitive H^+-uncaging at 0.11 Hz (denoted by *arrows*) in a small ROI (5 × 5 μm) positioned at the left end of the cell (see schematic diagram at top). The $[H^+]$-rise averaged in three downstream 15 × 15 μm ROIs is plotted versus time. Solid circles denote the mid-times between flash-events. The dashed lines illustrate the solution to a constant-source diffusion equation. (*B*) Protocol 2: simulation of brief sequence of flash-events in a 10 × 10 μm ROI positioned at the left end of the model-cell (*inset*). After inducing a 150 nM longitudinal H^+-gradient, flashing was stopped to allow the gradient to relax. Time courses of the rise and subsequent relaxation of $[H^+]_i$ in three downstream 15 × 15 μm ROIs are plotted as the continuous curves. Solid symbols indicate the expected timing of pH_i data acquisition during the relaxation phase.

phase can be simulated using a two-dimensional diffusion equation in a closed compartment, featuring a nonuniform initial condition given by the longitudinal pH_i-profile predicted after the final flash-event.

Local H^+-uncaging in isolated myocytes

The two acid-loading protocols were applied in experiments on rat myocytes superfused with HEPES-buffered NT containing 30 μM cariporide. The myocyte illustrated schematically in Fig. 4 *Ai* was exposed at 0.11 Hz to flash-events over a small 5 × 5 μm ROI set toward the left end of the cell (Protocol 1). Spatial pH_i data were acquired midway between flash-events, and these data points were interpolated to obtain $[H^+]_i$ time courses in three ROIs, as shown in Fig. 4 *Ai*. The delay of ~25 s between acidification in the proximal (*red*) and distal (*blue*) ROIs reflects a low mean value of D_H^{app}, estimated to be 10×10^{-7} cm^2/s in that particular cell (curve best-fit to data is plotted in black, Fig. 4 *Ai*). The goodness-of-fit between the model and experimental data was confirmed by plotting the measured longitudinal elevation of $[H^+]_i$ along a cell-wide ROI at different times after commencing the flash-sequence (Fig. 4 *Aii*), and superimposing this with model-predictions using the same mean value of D_H^{app} (*black lines*, Fig. 4 *Aii*).

In a different myocyte, a 10 × 10 μm ROI was exposed to a burst of six flash-events within a period of 12 s (Protocol 2), giving rise to an acute longitudinal pH_i nonuniformity. After the brief burst, the subsequent dissipation of the pH_i gradient is illustrated by the convergence of $[H^+]_i$ time courses measured in three ROIs (Fig. 4 *B*). When best-fitted with a diffusion equation, these data yielded a D_H^{app} of 5.5×10^{-7} cm^2/s.

The spatiotemporal behavior of H_i^+ in the sample experiments illustrated in Fig. 4 is consistent with that observed previously using a different technique where H^+-ions were introduced locally into a ventricular myocyte through a cell-attached micropipette. It is indicative of a diffusive process. The values derived for D_H^{app} are also within the range of previous estimates, suggesting that H_i^+-uncaging is a viable approach for investigating H_i^+-mobility. Results derived for D_H^{app} will be analyzed in more detail in a later section.

Local H^+-uncaging in myocyte cell-pairs

Photolytic uncaging of acid need not be limited to single cells. Fig. 5 illustrates the results of an experiment performed on a rat ventricular cell-pair superfused with HEPES-buffered NT containing 30 μM cariporide. A 5 × 5 μm region at the left end of one of the cells of the pair was exposed repetitively to flash-events (Protocol 1). As expected, the localized acid-load spread rightward along the proximal cell and permeated into the second cell across the gap junctional region (Fig. 5 *Ai*). This phenomenon has been demonstrated previously while using a micropipette to load acid directly into one cell of the pair (20). When the longitudinal elevation in $[H^+]_i$ was measured at different times

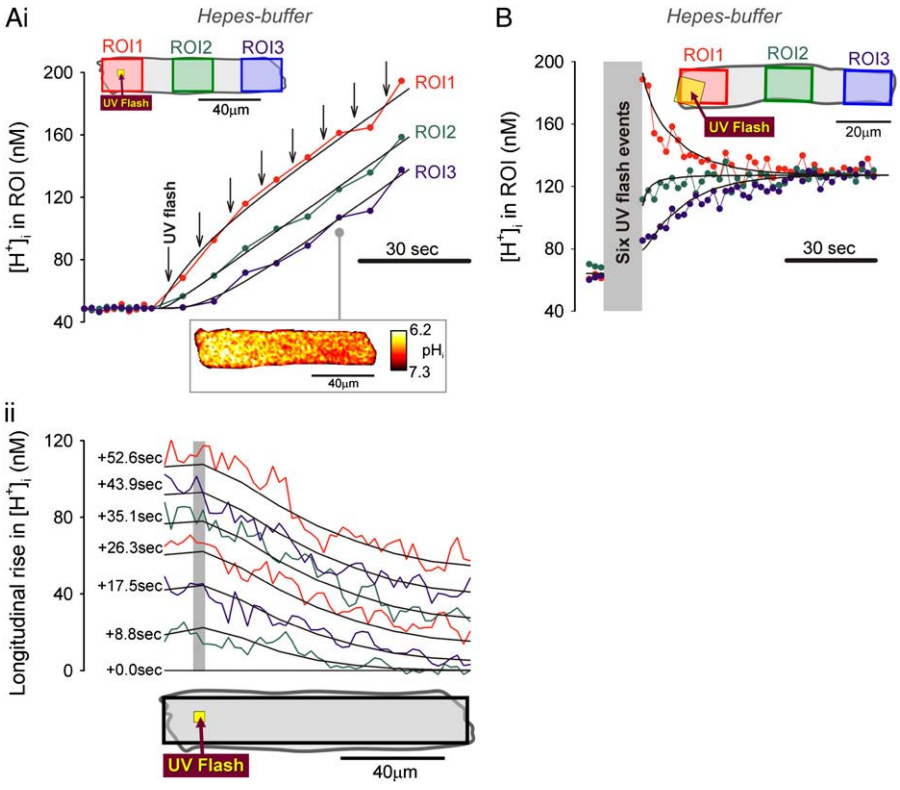

FIGURE 4 Local H^+-uncaging in an isolated myocyte (*Ai*). Protocol 1: rat myocyte, superfused with HEPES-buffered Tyrode containing 1 mM NBA and 30 μM cariporide. Repetitive flash-events (0.11 Hz) were applied to a 5 × 5μm ROI positioned at the left end of the cell. $[H^+]$ was averaged in three ROIs every 2.1 s (*colored circles*, coded to match the colored ROIs shown in schematic diagram at top); points have been interpolated to form continuous time courses. Superimposed black traces show best-fit solutions to a constant-source diffusion equation with a D_H^{app} of 10×10^{-7} cm^2/s. Inset shows a calibrated pH-map during acid-loading, taken at the time indicated. (*Aii*) Data from (*i*) are presented (*colored traces*) as longitudinal $[H^+]$-profiles at consecutive times, together with best-fit model predictions (*black lines*). The shaded vertical bar indicates the position of the H^+-uncaging site. (*B*) Protocol 2: rat myocyte, superfused with HEPES-buffered Tyrode containing 1 mM NBA and 30 μM cariporide. Six UV flash-events (0.5 Hz) were applied to a 15 × 15 μm ROI positioned toward the left end of the cell. After termination of flash sequence, the relaxation of $[H^+]$ averaged in three ROIs (traces color-coded to match ROIs shown in schematic diagram) is shown, along with superimposed best-fit model-predictions (*black traces*) for a D_H^{app} of 5.5×10^{-7} cm^2/s.

before and after commencement of the flash sequence, a large $[H^+]_i$-discontinuity was evident across the junction (Fig. 5 *Aii*), demonstrating that this region is rate-limiting for cell-to-cell H^+-ion transmission (20,31). Using a coupled two-compartment diffusive model with a constant local source for H^+-ions, and assuming H^+-ion reflection at all but the junctional boundaries, the data in Fig. 5 *A* were deconvoluted to give an estimate of the apparent proton permeability constant (P_H^{app}) across the junction. Fig. 5 *B* pools results for P_H^{app} from several H^+-uncaging experiments performed on myocyte cell-pairs. The mean P_H^{app} evaluated with this technique, $3.60(\pm 1.07) \times 10^{-4}$ cm/s, is similar to previous estimates of $2.03(\pm 0.66) \times 10^{-4}$ cm/s and $4.45(\pm 0.21) \times 10^{-4}$ cm/s measured using micropipette H^+-injection (20) or local weak acid/base microperfusion techniques (31). The presence of the gap junctional inhibitor, α-glycyrrhetinic acid (αGA) at 60 μM reduced P_H^{app} by 70–80% (Fig. 5 *B*), consistent with inhibition of H^+-passage through ventricular connexin channels (20).

Results of local H_i^+-uncaging in ventricular cell-pairs are thus comparable with those seen using other, more conventional acid-loading techniques (20,31). We conclude that H^+-uncaging from NBA is suitable for estimating cell-to-cell H^+-permeability as well as cytoplasmic H^+-mobility. We also conclude that inclusion of 1 mM NBA within cardiac myocytes does not influence the spatial movement of H^+ within the cell or its permeation through connexin channels.

pH_i-dependence of intracellular H^+-ion mobility

To resolve the pH_i-dependence of H^+-ion mobility, starting pH_i was manipulated uniformly to different levels before locally uncaging H^+ from NBA. Manipulation was achieved by prepulsing the cell with solutions containing the salt of a membrane-permeant weak acid (e.g., sodium acetate) or weak base (e.g., ammonium chloride), as described in the Methods section. On returning to normal Tyrode, pH_i respectively alkalinized and acidified (25). The pH_i was then stabilized at the new level by inhibiting sarcolemmal H^+-equivalent transport (see Methods).

H_i^+-uncaging experiments were repeated over a range of starting pH_i-values in the presence and absence of extrinsic carbonic buffer. Cumulative acid-loading (Protocol 1) in the presence of carbonic buffer is illustrated in Fig. 6 *A*. As with HEPES-buffer, $[H^+]_i$ increased fastest close to the site of H^+-release, whereas it rose more slowly in downstream regions. The estimated D_H^{app} for the cell shown in Fig. 6 *A* was 22×10^{-7} cm^2/s and was higher than that typically measured for cells superfused with HEPES-buffer.

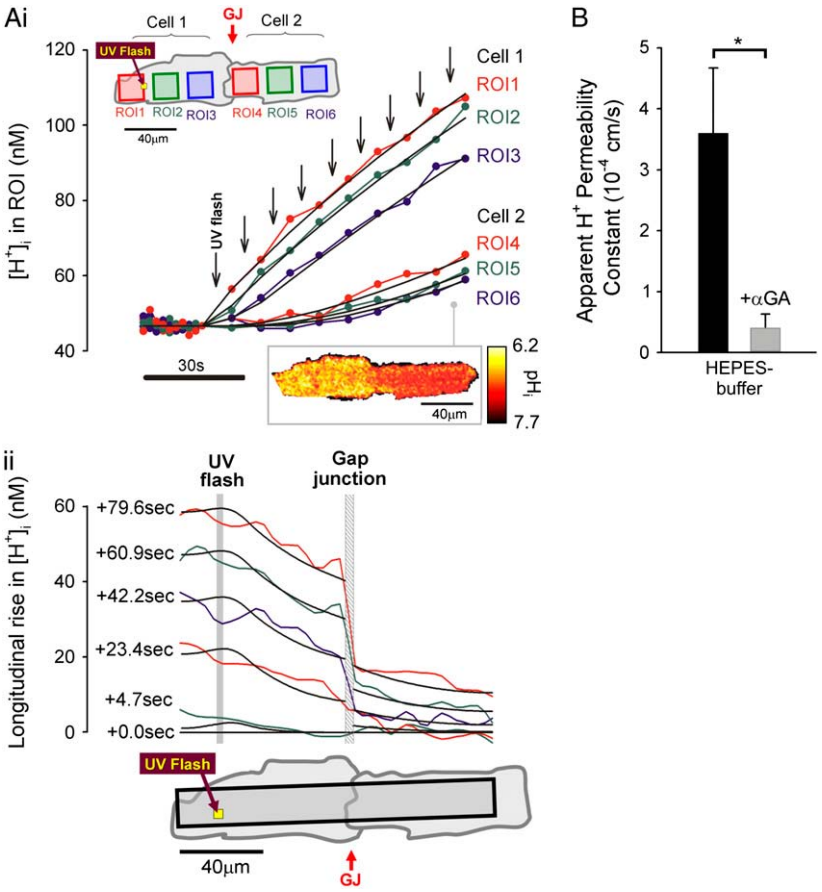

FIGURE 5 Local H^+-uncaging in a myocyte cell-pair (*Ai*). End-to-end rat myocyte cell-pair, superfused with HEPES-buffered Tyrode containing 1 mM NBA and 30 μM cariporide. Repetitive flash-events (0.11 Hz) were applied to a 5×5 μm ROI at the left end of the cell-pair. The color-coded time courses illustrate the cumulative rise in $[H^+]$. The superimposed black traces show best-fit solutions to a constant-source diffusion equation with a D_H^{app} of 9.5×10^{-7} cm^2/s and a P_H^{app} of 1.6×10^{-3} cm/s. Inset shows a calibrated pH-map during acid loading, taken at the time indicated. (*Aii*) Data from *i* are presented as longitudinal $[H^+]$-profiles at consecutive times, together with best-fit model-predictions. The vertical solid-gray bar indicates position of the acid-release site; diagonally lined bar highlights a discontinuity in the $[H^+]$-profile coincident with the gap junction. (*B*) Mean $\pm$SE for P_H^{app} measured with ($n = 6$) and without ($n = 7$) 60 μM α-glycerrhetinic acid (αGA) in superfusates, derived from experiments like that shown in Ai. Asterisk denotes significant difference ($P < 0.05$).

Values of D_H^{app} are plotted in Fig. 6 *B* versus the cell-averaged pH_i measured during the cumulative acid-load (see Methods). Values derived from cumulative H_i^+-loading (Protocol 1; *red, blue triangles*) as well as post-loading H_i^+-relaxation (Protocol 2; *open squares*) have been included. In some H^+-loading experiments performed in the presence of CO_2/HCO_3^- buffer (*green triangles*), 100 μM acetazolamide (ATZ) was added to superfusates, to retard carbonic buffer equilibration. This is normally catalyzed by endogenous carbonic anhydrase (CA) (32–34).

The data pooled in Fig. 6 *B* show that, for experiments performed under HEPES-buffered conditions, D_H^{app} decreases by about sixfold as mean pH_i decreases from 7.5 to 6.1. Results from the two acid-loading protocols were very similar when compared over a common pH_i-range. The relationship between pH_i and intrinsic D_H^{app} is similar to that deduced previously in rat and guinea pig ventricular myocytes (*dashed line*) using a dual microperfusion technique (12).

D_H^{app} in the presence of CO_2/bicarbonate-buffer was consistently higher than in HEPES, but its value still declined with pH_i (Fig. 6 *B*). Fig. 6 *C* plots the carbonic-induced increment of D_H^{app} over the whole pH_i range tested. It is largest at ~7.5 and decreases monotonically as pH_i falls. Interestingly, the decline is similar to that for intrinsic H^+-mobility. This is confirmed in Fig. 6 *D* which plots the fraction of D_H^{app} attributable to carbonic buffer alone. This fraction remains close to 30% over the pH_i range. Thus the pH_i-dependent properties of intrinsic and extrinsic H_i^+-mobility show virtually identical pH_i-sensitivity, resulting in near constant fractional contributions to H_i^+-mobility as pH_i is varied. The extrinsic component appeared to be dependent upon CA activity, as it was abolished by ATZ, leaving only the intrinsic component of D_H^{app}.

DISCUSSION

H_i^+-uncaging reveals pH-sensitivity of H_i^+-mobility

Photolytic uncaging of H^+-ions from intracellular NBA provides a unique way of examining H^+-ion dynamics in the cardiac ventricular myocyte. The technique has allowed us to assess the relative roles of intrinsic (non-CO_2) and extrinsic (carbonic) buffer, in the regulation of H_i^+-mobility. We find that the ability of both types of buffer to mediate intracellular H^+-ion movement declines about sixfold as intracellular pH decreases from 7.5 to 6.1. As pH_i falls, carbonic buffer's fractional contribution to D_H^{app} remains constant, at ~30%. A

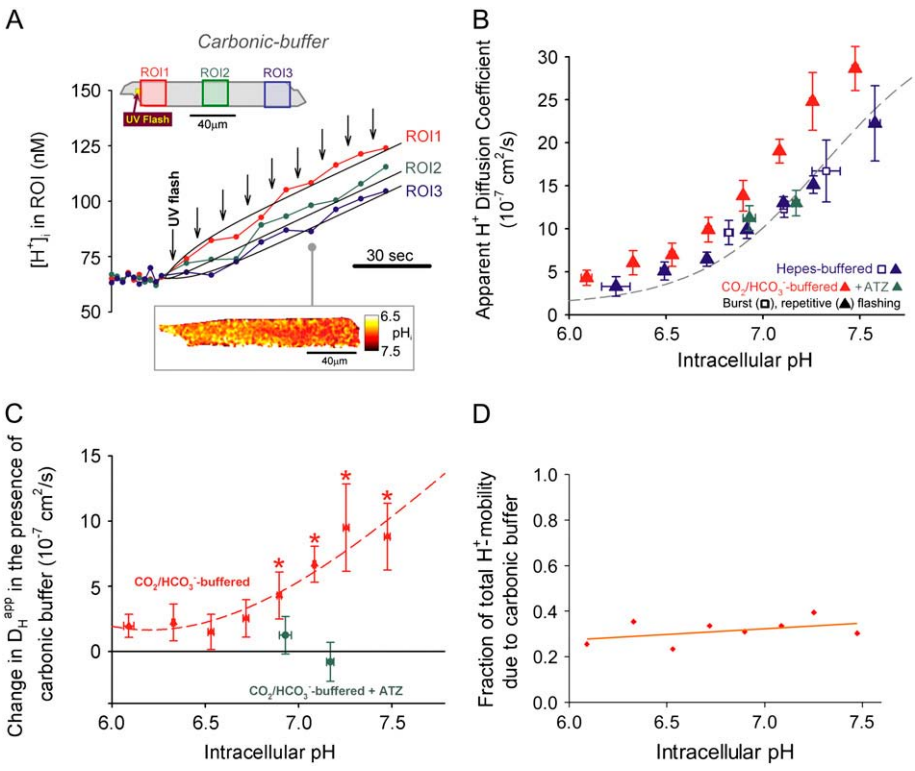

FIGURE 6 Intrinsic and extrinsic components of H_i^+-mobility are both pH-sensitive (*A*). A rat myocyte was superfused with CO_2/HCO_3^--buffered Tyrode containing 1 mM NBA and 30 μM cariporide. Repetitive flash-events (0.11 Hz) were applied to a 5 × 5μm ROI positioned at the left end of the cell (protocol 1). The colored circles show the rise of $[H^+]$ averaged in three ROIs (color-coded and positioned as shown in schematic diagram at top). Superimposed black traces show best-fit solutions to a constant-source diffusion equation with a D_H^{app} of 22 × 10^{-7} cm^2/s. Inset at bottom shows a calibrated pH-map of the cell during acid-loading, taken at time indicated. (*B*) Experiments using either protocol 1 (*solid triangles*) or 2 (*open squares*) for local H^+-uncaging (see text, and Fig. 3) in an isolated myocyte were performed from a range of starting pH_i-values, while superfusing the cell with HEPES-buffered (*blue symbols*) or CO_2/HCO_3^--buffered (*red symbols*) solution. Starting pH_i was preset using a weak acid/base prepulse technique (see Methods). Blue triangles, n = 4, 11, 34, 46, 98, 42, 25; blue open squares, n = 19, 22, 5; red triangles, n = 7, 10, 11, 10, 18, 37, 9, 8. The dashed line illustrates the pH_i-dependence of D_H^{app} measured previously using a different technique (12). All red data-points are significantly different from the dashed line (z-test, 95% confidence level). In some experiments, 100 μM ATZ was added to CO_2/HCO_3^- superfusates to block carbonic anhydrase (*green triangles*, n = 17,19). These data points were not significantly different from the dashed line (*z*-test, 95% confidence level). (*C*) The change in D_H^{app} in the presence of CO_2/HCO_3^- buffer is plotted as a function of pH_i (*red symbols*, without ATZ; *green symbols*, with ATZ). The dashed red line represents the difference between the best-fit sigmoidal curve to the D_H^{app} data in the presence and absence of carbonic buffer. (*D*) The fraction of D_H^{app} that is measured in CO_2/HCO_3^--buffered solution (in the absence of ATZ) that is attributable to carbonic (i.e., nonintrinsic) buffering. This fraction is close to 0.3 over the entire pH_i-range studied. Data points in panels *B* and *C* show mean ± SE.

comparable pH_i-sensitivity of intrinsic D_H^{app} has been reported previously for rat and guinea pig myocytes (12), using a radically different technique (local pH_i-displacement with membrane-permeant weak acid or base). In that work, however, experiments were not performed in the presence of carbonic buffer so the pH_i-sensitivity of extrinsic H_i^+-mobility could not be explored.

The physiological benefit of a decline in D_H^{app} with pH_i is unclear, but it may represent a strategy for slowing the spatial spread of a local intracellular acid insult, both within a cell and within a multicellular region. Intracellular acid-overload is potentially damaging to cardiac tissue, as it is associated with intracellular Ca^{2+}-overload (35,36), leading to electrical and mechanical malfunction (6,8,9). Slow spatial spread of H^+-ions may, for example, facilitate their local removal via sarcolemmal transport mechanisms, thus restricting their global impact on the myocardium.

The pH_i-dependence of D_H^{app} revealed using H^+-uncaging, indicates that in the presence of CO_2/HCO_3^-, total D_H^{app} at pH_i 6.1 is $\sim 4\times10^{-7}$ cm^2/s. This value is nearly 300-fold lower than H^+-mobility in water (at 37°C, $D_H = 12 \times 10^{-5}$ cm^2/s). Such low mobility predicts that acidosis will predispose intracellular pH to spatial non-uniformity. Indeed such non-uniformity at low pH_i has already been observed in the ventricular myocyte during stimulation of sarcolemmal Na^+-H^+ exchange (13). Intracellular pH nonuniformity induced by stimulation of H^+-equivalent membrane transport has also been observed in epithelial cells (15), and in invertebrate and mammalian neurons (37,38). It seems likely that, in these cell-types, a similar decline of H_i^+-mobility with pH_i will contribute to the generation of local pH_i microdomains.

Flash-photolysis of NBA: a novel experimental tool

NBA appears suitable for intracellular proton uncaging. In the mammalian ventricular myocyte, its toxicity is minimal at the doses used. In the absence of UV flashing, 1 mM NBA had no effect on diastolic Ca_i^{2+} or on the time course and amplitude of an electrically-evoked Ca^{2+}-transient. It also had no direct effect on cellular contraction, although an unexplained slowing of the later stage of relaxation was sometimes detected. Most importantly, 1 mM NBA had no effect on the mechanisms of spatial pH_i regulation, as evidenced by a lack of effect on estimates of H_i^+-mobility (D_H^{app}) and cell-to-cell H^+-permeability (P_H^{app}). Flash-photolysis of intracellular NBA should therefore be an important new tool in the study of pH_i regulation.

Advantages of the technique

The technique can be used to produce whole-cell as well as local pH_i-changes (cf. Fig. 2 with 4). Experiments need not be limited to single-cells but can be performed equally well on cell-pairs, and may also be suitable for tissue or whole-organ studies. UV flashing in the absence of NBA had no effect on pH_i (Fig. 2 *D*), eliminating the possibility of an acid-source other than NBA, or of an artifactual UV-interaction with intracellular carboxy-SNARF. We assessed the technique as an alternative to previous approaches for inducing pH_i nonuniformity. These have comprised localized myocyte-exposure to weak acids or bases (17,18,31) or localized acid-loading via a patch pipette (11,14,16,20). UV flash-photolysis of caged-H^+ compounds was a simpler technique to use, with a much higher success rate experimentally. Furthermore, unlike the other two acid-loading techniques, the size, speed, and magnitude of intracellular loading could readily be varied during an experiment by adjusting the UV laser intensity.

Intracellular NBA photolysis has previously been tested in snail neurons (19) but the physicochemical properties of the technique were not quantified. In this work we monitored pH_i ratiometrically and estimated the magnitude of local and whole-cell pH_i-changes. When exposed to a dose of UV light, NBA releases a quantity of acid (Fig. 2 *C*) that is dependent on the laser intensity (Fig. 2 *E*). At 100% laser intensity (20 mW) the photolytic efficiency is very high, reaching 80% (i.e., during a single flash, 0.80 mM acid was released per 1 mM NBA). This is a considerably higher efficiency than that attained with other caged-H^+ compounds such as 4-formyl-6-methoxy-3-nitrophenoxyacetic acid (39).

Since 2-nitrosobenzoic acid, the product of NBA photolysis, has a low pK, it will fully dissociate into H^+ and 2-nitrosobenzoate in the physiological pH range and produce an acid-load that is independent of pH_i. H^+-ions are therefore trapped intracellularly, and the trapping becomes cumulative during a series of flash-events (Fig. 3). In this respect, NBA is better than a substance such as 2-hydroxyphenyl 1-(2-nitrophenyl)ethyl phosphate (40) which has a pK value near 5, and therefore does not fully dissociate, so that its acid-delivery will vary with pH_i. Its anionic conjugate-base will also contribute to cytoplasmic H^+-buffering capacity.

Owing to the high membrane-permeability of NBA, its inclusion in the superfusate effectively clamps its intracellular concentration. The compound is also rapidly replenished after photolysis and was never a limiting factor in this work (cf. the linearity of the relationship shown in Fig. 2 *E* between the concentration of acid uncaged and that of NBA). Some previously used H^+-donors, e.g., 4-formyl-6-methoxy-3-nitrophenoxyacetic acid (39) are poorly membrane-permeant and therefore less suitable.

Disadvantages of the technique

These are fourfold. Firstly, as alluded to above, prolonged exposure to intense UV light causes cell damage, but we have defined experimental protocols that appear to minimize this. Secondly, NBA appeared to be cytotoxic at concentrations as high as 10 mM, although such effects were minimal at 1 mM. We have not specifically examined the nature of NBA-toxicity but, at high concentration, NBA has tissue-fixative properties. In view of this, it may be prudent to limit

its dosage to no more than 1 mM. Thirdly, photolysis of NBA will cause intracellular accumulation of nitrosobenzoate and, at high concentration, this will impose an untoward osmotic stress on the cell. For modest whole-cell acid-loads or for spatially localized uncaging maneuvers, this is unlikely to present a serious problem. For example, a whole cell acid-load of 0.5 pH_i units would release ~25 mM nitrosobenzoate, causing an increase of intracellular osmolarity of ~8%, which will induce osmotic swelling. This level of osmotic loading is well tolerated by cardiac myocytes. Indeed acid-loading by any experimental technique, or indeed metabolically by the cell itself, is likely to be accompanied by a comparable osmotic load, as protons must be added with an equivalent anionic charge, much of which will be osmotically active. The fact, however, that nitrosobenzoate is membrane impermeant, and therefore cannot escape from the cell, should be borne in mind when contemplating prolonged NBA-uncaging experiments. Fourthly, because it is so membrane permeant, NBA may well gain access to intracellular organelles. The uncaging procedure may therefore release H^+-ions directly into the sarcoplasmic reticulum or into mitochondria, in addition to the cytoplasm. In our present single-photon excitation system, this effect may be amplified by photolytic H^+-release within the cones of UV illumination above and below the confocal plane (this latter problem would be greatly reduced by multiphoton excitation exclusively in the confocal plane). Where H^+-ion release into organelles is considered to be a potential problem, it may be prudent to compare results with those obtained using a cell-attached acid-filled micropipette (where H^+-ions initially access only the cytoplasm). In the present determinations of intrinsic D_H^{app}, for example, it is unlikely that possible H^+-release into organelles was significantly interfering with measurements of cytoplasmic H^+-movement, as D_H^{app} was comparable when measured by both techniques. Overall, when reviewing the use of intracellular NBA as an experimental tool it would seem that, for many experimental purposes, the advantages far outweigh the disadvantages.

MECHANISM OF pH-SENSITIVE H_i^+-MOBILITY

Intrinsic H_i^+-mobility

We have shown previously that the pH_i-dependence of intrinsic D_H^{app} is consistent with two pooled populations of intrinsic buffer (12). One appears to have very low or zero mobility, most likely represented by buffer sites on intracellular proteins. The other appears to be more mobile, represented by lower molecular weight molecules such as the histidyl dipeptides (100–200 Da) that are prevalent in many tissues, including heart (41) and skeletal muscle (42). As described in the Introduction, H_i^+-mobility is dependent on spatial H^+-shuttling by these mobile buffer molecules. They are estimated to have a pooled diffusion coefficient, D_{mob}, equal to 49.9×10^{-7} cm^2/s (12). Since the intrinsic buffers equilibrate rapidly (25), the apparent diffusion coefficient (D_H^{app}) can be described using the equation:

$$D_H^{app} = \frac{D_{mob} \times \beta_{mob}}{\beta_{mob} + \beta_{fix}}, \quad (1)$$

where D_{mob} and β_{mob} denote the intrinsic mobile buffer diffusion coefficient and capacity respectively, and where β_{fix} denotes the intrinsic fixed buffer capacity (11,43). On this scheme, the pH_i-dependence of intrinsic D_H^{app} is consistent with a pH_i-dependence of β_{mob} and β_{fix}, the former having a mean pK of ~7.48 and the latter a much lower mean pK of 6.40 (12). Thus as pH_i decreases from a resting value of ~7.1, β_{mob} also decreases as it becomes saturated with H^+-ions, whereas β_{fix} increases as ambient pH approaches its pK. The mobile fraction of intrinsic buffering thus decreases, resulting in a fall of H_i^+-mobility.

Extrinsic H_i^+-mobility

Comparison with previous work

Introducing carbonic buffer into a rat myocyte increased D_H^{app} by ~50% (i.e., the extrinsic component of D_H^{app} is ~30% of total D_H^{app}). Although an increase was found in previous work on guinea-pig and rabbit ventricular myocytes, it appeared to be much larger (two- to fivefold). Some of this discrepancy may represent species differences, but there are other possible explanations. Firstly, initial work with CO_2/HCO_3^- buffer (14) estimated D_H^{app} from the time delay for H^+-ion diffusion down a cell, when injected locally from a micropipette. Unlike more recent analyses (16,29), the specific geometry of each cell was not taken into account (myocyte geometry was standardized as rectangular). As a result, errors in estimating D_H^{app} may have arisen, particularly when the time delay was small. Secondly, most previous work did not acknowledge the pH_i-dependence of D_H^{app}. The graph shown in Fig. 6 *B* illustrates that carbonic buffer's contribution is 2×10^{-7} cm^2/s at pH_i 6.1, rising to nearly 10×10^{-7} cm^2/s at pH_i 7.5. The intrinsic contribution varies from $2.5–22 \times 10^{-7}$ cm^2/s over the same range (Fig. 6 *A*), which encompasses the averaged values for intrinsic D_H^{app} reported previously (typically $\sim 8 \times 10^{-7}$ cm^2/s). Thus, if H_i^+-mobility values were not compared at a common pH_i, the contribution of carbonic buffer would appear to range from 10% to 500%. Clearly the procedure of using a common pH_i value when comparing D_H^{app} values must now be adopted. A final reason for differing estimates of carbonic buffer's contribution to H_i^+-mobility may be its slow kinetics, which permit the buffer to mediate slow, but not fast, H_i^+-shuttling reactions. We return to this point in a later section.

Extrinsic H_i^+-mobility constrained by fixed buffers and $[HCO_3^-]_i$

HCO_3^- anions, in concert with CO_2, act as mobile buffers within the cell, shuttling H^+-ions spatially (14,15). Like

other mobile buffers, HCO_3^- ions must compete with fixed intrinsic buffers for H^+-ion binding. Given that β_{fix} rises steeply as pH_i falls (12,16), part of the observed decline in the effectiveness of the extrinsic shuttle at low pH_i (Fig. 6 *C*) can be attributed to increased competition from fixed buffers. This would predict a 1.7-fold decline in extrinsic H^+-mobility, rather than the fivefold decline actually observed (Fig. 6 *C*). Thus other factors must also play a role.

Assuming that CO_2 is freely permeant across the sarcolemma, so that $[CO_2]_i$ is clamped by a constant extracellular $[CO_2]$, carbonic buffering capacity at equilibrium can be expressed as a function of intracellular bicarbonate concentration (24):

$$\beta_{carb} = \ln(10) \times [HCO_3^-]_i = \ln(10) \times [HCO_3^-]_o \times 10^{pH_i - pH_o}, \quad (2)$$

where subscripts *i* and *o* denote the intracellular and extracellular compartments, respectively. Equation 1 has previously been modified to describe the H_i^+-mobility constant in the presence of carbonic buffer (14) by including two extra terms, β_{carb} and D_{carb} (the effective diffusion coefficient of carbonic buffer, a term lumped for the individual diffusion coefficients of intracellular CO_2 and HCO_3^-, the constituents of carbonic buffer):

$$D_H^{app} = \frac{D_{mob} \times \beta_{mob} + D_{carb} \times \beta_{carb}}{\beta_{mob} + \beta_{carb} + \beta_{fix}}. \quad (3)$$

Assuming the cell remains fully open to CO_2, much of the pH_i-dependence of extrinsic H_i^+-mobility can be explained by a fall in $[HCO_3^-]_i$, and hence a fall of β_{carb} as pH_i declines. Over the pH_i range from 7.5 to 6.1, β_{carb} at equilibrium falls 25-fold. This would be more than sufficient to account for the decline in the extrinsic component of H_i^+-mobility (Fig. 6 *C*). During intracellular acidosis, H^+-movement via the carbonic shuttle is therefore likely to be constrained by the H^+-binding capacity of fixed buffers, and by the availability of intracellular bicarbonate.

Extrinsic H_i^+-mobility also constrained by slow buffer-kinetics

Although extrinsic H_i^+-mobility will be influenced by $[HCO_3^-]_i$, quantifying this effect is not straightforward. Eq. 3 can be used to predict D_H^{app} in the presence of carbonic buffer, provided the effective value for β_{carb} is known. In this work, net H_i^+-movement was observed over periods of 1–2 min. Unfortunately, on this timescale, β_{carb} cannot reliably be estimated from Eq. 2, as the CO_2/HCO_3^- buffer system may not be close to equilibrium. CO_2-hydration is slow and only moderately accelerated in cardiomyocytes by endogenous CA (34). As a result, intracellular carbonic buffering is also slow, often taking minutes to equilibrate. During this period, the effective value of β_{carb} may be significantly less than its equilibrium value. This raises difficulties for computing D_H^{app}.

By assigning a value to D_{carb}, Eq. 3 can be used to explore the effective value of β_{carb} during spatial H_i^+-movement. After correcting for temperature and macromolecular crowding in the cytosolic environment, the intracellular diffusion coefficients for CO_2 and HCO_3^- (the constituents of carbonic buffer) have been estimated as 11 and 7.7×10^{-6} cm^2/s, respectively (29). D_{carb} can be represented by the lower of the two coefficients, i.e., 7.7×10^{-6} cm^2/s. Best-fitting the data in Fig. 6 *B* with Eq. 3 yields estimates for β_{carb}, which rise from around 1 mM at pH 6.1 to 4 mM at pH 7.5. These are considerably smaller than the equilibrium values predicted from Eq. 2 (2.5 and 63 mM, respectively). The low effective values for β_{carb} are therefore suggestive of an out-of-equilibrium state, whereby carbonic buffer contributes only a fraction of its full capacity to the shuttling of intracellular H^+-ions. The exact value of this fraction will depend on the buffer's catalytic acceleration by CA, the magnitude of the spatial acid-flux, and movements of CO_2 across the sarcolemma. This conclusion is reinforced by the observation that extrinsic H_i^+-mobility disappears entirely when CA is inhibited by acetazolamide (Fig. 6 *B*, *green triangles*).

The above calculations suggest that, during the intracellular acid-loading rate used in this study (~15 mM/min averaged over the cell), the effective value of β_{carb} was reduced by 2.5–15-fold from its equilibrium value. Much larger spatial acid-fluxes (~100 mM/min) have been induced previously in experiments involving partial exposure of a myocyte to ammonium chloride (18). In those experiments, the presence of carbonic buffer had virtually no effect on H_i^+-mobility, suggesting the effective value of β_{carb} may have fallen to near zero.

The ability of the CO_2/HCO_3^--shuttle to mediate H_i^+-movement in the cardiac myocyte will therefore be limited, not only by fixed buffers and the availability of intracellular bicarbonate, but also by the extrinsic buffer's slow kinetics. When spatial pH_i nonuniformity is large, resulting in high intracellular H^+-traffic, the buffer's fractional contribution will be reduced. The present estimate of 30% should therefore be viewed in the context of the size of the underlying spatial acid-flux. Significant differences in flux magnitude may account for reported differences in the buffer's contribution to H_i^+-mobility (this work; (14,16,18)), and in its ability to minimize pH_i nonuniformity (14–16,38).

Because of uncertainty regarding the effective value of β_{carb} during H_i^+-shuttling, the mechanism for pH-dependent extrinsic H_i^+-mobility has yet to be modeled quantitatively. Even if carbonic buffer is significantly out-of-equilibrium, as seems likely during some local H_i^+-movement, the restricted availability of intracellular HCO_3^- during acidosis will be an important constraining factor. An additional factor may be a pH_i-sensitivity of the CA enzyme, as this regulates the speed of buffer equilibration (32,34). CA isoforms I and II are known to be pH-sensitive (44), but the isoforms responsible for facilitating intracellular H^+-ion movement in the cardiac myocyte have yet to be identified.

CONCLUSIONS

Flash-photolysis of intracellular NBA provides a convenient and novel tool for displacing intracellular pH. The approach is simple to implement and need not be restricted to single-cell preparations. It should prove useful in cell-types less amenable to conventional methods of local acid-injection. Using the method, we have demonstrated that, in ventricular cells, both extrinsic (carbonic) and intrinsic buffers regulate intracellular H^+-ion movement. With these experimental protocols, extrinsic buffer accounts for ~30% of H_i^+-mobility over a wide pH_i-range. The fact that this component relies upon the activity of CA indicates the important role of this enzyme in spatial pH_i regulation. The remaining 70% of H_i^+-movement is mediated by intrinsic mobile buffers. A key finding is that both extrinsic and intrinsic H_i^+-mobility are severely reduced during intracellular acidosis. This will compromise the spatial uniformity of pH_i, particularly when sarcolemmal H^+-equivalent extruders are stimulated (13). The physiological consequences of spatial pH_i nonuniformity are only now being investigated, but they are likely to include a spatial disruption of both Ca_i^{2+}-signaling (45,46) and contraction (46). Severe intracellular acidosis in the cardiac myocyte may thus present a window of vulnerability in the spatial coordination of cell function.

The authors thank Mr. Philip Cobden for excellent technical assistance.

This work was supported by a British Heart Foundation Program grant to R.V.J, and a MERIT award from the National Institutes of Health to K.W.S. (5R37HL042873).

REFERENCES

1. Bountra, C., K. Kaila, and R. D. Vaughan-Jones. 1988. Effect of repetitive activity upon intracellular pH, sodium and contraction in sheep cardiac Purkinje fibres. *J. Physiol.* 398:341–360.
2. Elliott, A. C., G. L. Smith, and D. G. Allen. 1994. The metabolic consequences of an increase in the frequency of stimulation in isolated ferret hearts. *J. Physiol.* 474:147–159.
3. Ellis, D., and R. C. Thomas. 1976. Microelectrode measurement of the intracellular pH of mammalian heart cells. *Nature.* 262:224–225.
4. Bountra, C., and R. D. Vaughan-Jones. 1989. Effect of intracellular and extracellular pH on contraction in isolated, mammalian cardiac muscle. *J. Physiol.* 418:163–187.
5. Komukai, K., F. Brette, C. Pascarel, and C. H. Orchard. 2002. Electrophysiological response of rat ventricular myocytes to acidosis. *Am. J. Physiol. Heart Circ. Physiol.* 283:H412–H422.
6. Fabiato, A., and F. Fabiato. 1978. Effects of pH on the myofilaments and the sarcoplasmic reticulum of skinned cells from cardiace and skeletal muscles. *J. Physiol.* 276:233–255.
7. Garlick, P. B., G. K. Radda, and P. J. Seeley. 1979. Studies of acidosis in the ischaemic heart by phosphorus nuclear magnetic resonance. *Biochem. J.* 184:547–554.
8. Orchard, C. H., and J. C. Kentish. 1990. Effects of changes of pH on the contractile function of cardiac muscle. *Am. J. Physiol.* 258:C967–C981.
9. Orchard, C. H., and H. E. Cingolani. 1994. Acidosis and arrhythmias in cardiac muscle. *Cardiovasc. Res.* 28:1312–1319.
10. Vaughan-Jones, R. D., K. W. Spitzer, and P. Swietach. 2005. Spatial aspects of intracellular pH regulation in heart muscle. *Prog. Biophys. Mol. Biol.* 90:207–224.
11. Vaughan-Jones, R. D., B. E. Peercy, J. P. Keener, and K. W. Spitzer. 2002. Intrinsic H^+ ion mobility in the rabbit ventricular myocyte. *J. Physiol.* 541:139–158.
12. Swietach, P., and R. D. Vaughan-Jones. 2005. Relationship between intracellular pH and proton mobility in rat and guinea-pig ventricular myocytes. *J. Physiol.* 566:793–806.
13. Swietach, P., and R. D. Vaughan-Jones. 2005. Spatial regulation of intracellular pH in the ventricular myocyte. *Ann. N. Y. Acad. Sci.* 1047:271–282.
14. Spitzer, K. W., R. L. Skolnick, B. E. Peercy, J. P. Keener, and R. D. Vaughan-Jones. 2002. Facilitation of intracellular H^+ ion mobility by CO_2/HCO_3^- in rabbit ventricular myocytes is regulated by carbonic anhydrase. *J. Physiol.* 541:159–167.
15. Stewart, A. K., C. A. Boyd, and R. D. Vaughan-Jones. 1999. A novel role for carbonic anhydrase: cytoplasmic pH gradient dissipation in mouse small intestinal enterocytes. *J. Physiol.* 516:209–217.
16. Zaniboni, M., P. Swietach, A. Rossini, T. Yamamoto, K. W. Spitzer, and R. D. Vaughan-Jones. 2003. Intracellular proton mobility and buffering power in cardiac ventricular myocytes from rat, rabbit, and guinea pig. *Am. J. Physiol. Heart Circ. Physiol.* 285:H1236–H1246.
17. Spitzer, K. W., P. R. Ershler, R. L. Skolnick, and R. D. Vaughan-Jones. 2000. Generation of intracellular pH gradients in single cardiac myocytes with a microperfusion system. *Am. J. Physiol. Heart Circ. Physiol.* 278:H1371–H1382.
18. Swietach, P., C. H. Leem, K. W. Spitzer, and R. D. Vaughan-Jones. 2005. Experimental generation and computational modeling of intracellular pH gradients in cardiac myocytes. *Biophys. J.* 88:3018–3037.
19. Schwiening, C. J. 2004. Rapid regionally restricted pH_i shifts in neurons induced by the UV photolysis of 2-nitrobenzaldehyde. *J. Physiol.* 555P:D1.
20. Zaniboni, M., A. Rossini, P. Swietach, N. Banger, K. W. Spitzer, and R. D. Vaughan-Jones. 2003. Proton permeation through the myocardial gap junction. *Circ. Res.* 93:726–735.
21. Haugland, R. P. 2002. Handbook of Fluorescent Probes and Research Products. Molecular Probes, Eugene, OR.
22. Thomas, J. A., R. N. Buchsbaum, A. Zimniak, and E. Racker. 1979. Intracellular pH measurements in Ehrlich ascites tumor cells utilizing spectroscopic probes generated in situ. *Biochemistry.* 18:2210–2218.
23. Saxena, A. M., J. B. Udgaonkar, and G. Krishnamoorthy. 2005. Protein dynamics control proton transfer from bulk solvent to protein interior: a case study with a green fluorescent protein. *Protein Sci.* 14:1787–1799.
24. Roos, A., and W. F. Boron. 1981. Intracellular pH. *Physiol. Rev.* 61: 296–434.
25. Leem, C. H., D. Lagadic-Gossmann, and R. D. Vaughan-Jones. 1999. Characterization of intracellular pH regulation in the guinea-pig ventricular myocyte. *J. Physiol.* 517:159–180.
26. Scholz, W., U. Albus, L. Counillon, H. Gogelein, H. J. Lang, W. Linz, A. Weichert, and B. A. Scholkens. 1995. Protective effects of HOE642, a selective sodium-hydrogen exchange subtype 1 inhibitor, on cardiac ischaemia and reperfusion. *Cardiovasc. Res.* 29:260–268.
27. Yamamoto, T., P. Swietach, A. Rossini, S. H. Loh, R. D. Vaughan-Jones, and K. W. Spitzer. 2005. Functional diversity of electrogenic Na^+-HCO_3^- cotransport in ventricular myocytes from rat, rabbit and guinea pig. *J. Physiol.* 562:455–475.
28. Sun, B., C. H. Leem, and R. D. Vaughan-Jones. 1996. Novel chloride-dependent acid loader in the guinea-pig ventricular myocyte: part of a dual acid-loading mechanism. *J. Physiol.* 495:65–82.
29. Swietach, P., M. Zaniboni, A. K. Stewart, A. Rossini, K. W. Spitzer, and R. D. Vaughan-Jones. 2003. Modelling intracellular H^+ ion diffusion. *Prog. Biophys. Mol. Biol.* 83:69–100.
30. Abbruzzetti, S., E. Crema, L. Masino, A. Vecli, C. Viappiani, J. R. Small, L. J. Libertini, and E. W. Small. 2000. Fast events in protein

folding: structural volume changes accompanying the early events in the N→I transition of apomyoglobin induced by ultrafast pH jump. *Biophys. J.* 78:405–415.

31. Swietach, P., and R. D. Vaughan-Jones. 2004. Novel method for measuring junctional proton permeation in isolated ventricular myocyte cell pairs. *Am. J. Physiol. Heart Circ. Physiol.* 287:H2352–H2363.
32. Geers, C., and G. Gros. 2000. Carbon dioxide transport and carbonic anhydrase in blood and muscle. *Physiol. Rev.* 80:681–715.
33. Knuppel-Ruppert, A. S., G. Gros, W. Harringer, and H. P. Kubis. 2000. Immunochemical evidence for a unique GPI-anchored carbonic anhydrase isozyme in human cardiomyocytes. *Am. J. Physiol. Heart Circ. Physiol.* 278:H1335–H1344.
34. Leem, C. H., and R. D. Vaughan-Jones. 1998. Out-of-equilibrium pH transients in the guinea-pig ventricular myocyte. *J. Physiol.* 509:471–485.
35. Gambassi, G., R. G. Hansford, S. J. Sollott, B. A. Hogue, E. G. Lakatta, and M. C. Capogrossi. 1993. Effects of acidosis on resting cytosolic and mitochondrial Ca^{2+} in mammalian myocardium. *J. Gen. Physiol.* 102:575–597.
36. Kaila, K., and R. D. Vaughan-Jones. 1987. Influence of sodium-hydrogen exchange on intracellular pH, sodium and tension in sheep cardiac Purkinje fibres. *J. Physiol.* 390:93–118.
37. Schwiening, C. J., and D. Willoughby. 2002. Depolarization-induced pH microdomains and their relationship to calcium transients in isolated snail neurones. *J. Physiol.* 538:371–382.
38. Willoughby, D., and C. J. Schwiening. 2002. Electrically evoked dendritic pH transients in rat cerebellar Purkinje cells. *J. Physiol.* 544: 487–499.
39. Janko, K., and J. Reichert. 1987. Proton concentration jumps and generation of transmembrane pH-gradients by photolysis of 4-formyl-6-methoxy-3-nitrophenoxyacetic acid. *Biochim. Biophys. Acta.* 905: 409–416.
40. Khan, S., F. Castellano, J. L. Spudich, J. A. McCray, R. S. Goody, G. P. Reid, and D. R. Trentham. 1993. Excitatory signaling in bacterial probed by caged chemoeffectors. *Biophys. J.* 65:2368–2382.
41. O'Dowd, J. J., D. J. Robins, and D. J. Miller. 1988. Detection, characterization, and quantification of carnosine and other histidyl derivatives in cardiac and skeletal muscle. *Biochim. Biophys. Acta.* 967: 241–249.
42. Abe, H. 2000. Role of histidine-related compounds as intracellular proton buffering constituents in vertebrate muscle. *Biochemistry (Mosc.).* 65:757–765.
43. Irving, M., J. Maylie, N. L. Sizto, and W. K. Chandler. 1990. Intracellular diffusion in the presence of mobile buffers. Application to proton movement in muscle. *Biophys. J.* 57:717–721.
44. Khalifah, R. G. 1971. The carbon dioxide hydration activity of carbonic anhydrase. I. Stop-flow kinetic studies on the native human isoenzymes B and C. *J. Biol. Chem.* 246:2561–2573.
45. Dilworth, E. L., P. Swietach, and R. D. Vaughan-Jones. 2006. Local control of ventricular Ca^{2+}-signalling by intracellular pH. Biophysical Society 50th Annual Meeting. 2006:1552.
46. Spitzer, K. W., and R. D. Vaughan-Jones. 2006. Regional intracellular acidosis in ventricular myocytes creates spatial gradients in Ca^{2+} transients. Biophysical Society 50th Annual Meeting. 73A.